Steering-enhanced quantum metrology using superpositions of quantum channels

Kuan-Yi Lee,[1, *] Jhen-Dong Lin,[1, *] Adam Miranowicz,[2, 3]
Franco Nori,[2, 4, 5] Huan-Yu Ku,[1, 2, †] and Yueh-Nan Chen[1, 2, ‡]

[1]*Department of Physics and Center for Quantum Frontiers of Research &
Technology (QFort), National Cheng Kung University, Tainan 701, Taiwan*
[2]*Theoretical Quantum Physics Laboratory, RIKEN Cluster for Pioneering Research, Wako-shi, Saitama 351-0198, Japan*
[3]*Institute of Spintronics and Quantum Information, Faculty of Physics, Adam Mickiewicz University, 61-614 Poznań, Poland*
[4]*RIKEN Center for Quantum Computing, Wako, Saitama 351-0198, Japan*
[5]*Department of Physics, The University of Michigan, Ann Arbor, 48109-1040 Michigan, USA*

Quantum steering is an important correlation in quantum information theory. A recent work [Nat. Commun. 12, 2410 (2021)] showed that quantum steering is also beneficial to quantum metrology. Here, we extend the exploration of this steering-enhanced quantum metrology from a noiseless regime to a superposition of noisy phase shifts in quantum channels. As concrete examples, we consider a control system that manipulates the target to pass through superpositions of either dephased or depolarized phase shifts. We show that the deterioration due to the noise can be mitigated by selecting the outcome on the control system. Further, we also implement proof-of-principle experiments for a superposition of the dephased phase shifts on a IBM Quantum computer. Our experimental results agree with the noise simulations that take into account the intrinsic errors of the device.

I. INTRODUCTION

Quantum theory allows one party (Alice) to remotely steer another party (Bob) by her choice of measurements. Such a quantum phenomenon is called quantum (or Einstein–Podolsky–Rosen) steering. Although the concept of quantum steering was first proposed by Schrödinger in early 20th century [1], its information-theoretic description was formulated only quite recently, i.e., in 2007 [2–4]. Nowadays, not only many experimental realizations [5–10] of quantum steering have been demonstrated, but also various theoretical applications, such as quantum foundations [11–17], and one-sided device-independent quantum information tasks [18–24] have been proposed.

Apart from the information-theoretic formulation, Reid *et al.* [25, 26] investigated quantum steering from the viewpoint of the local uncertainty principle [27]. The idea is that the complementary relations between a pair of Bob's non-commutative observables could violate the Heisenberg's limit if the correlation shared by Alice and Bob is steerable. In other words, the local uncertainty principle can be regarded as a criterion of steering. Recently, Yadin *et al.* [28] showed that Reid's criterion can be extended to the domain of quantum metrology [29–33], where Bob aims to estimate an unknown phase shift θ generated by a Hamiltonian H. Their proposal has also been implemented in an optical system by Gianani *et al.* [34]. A main result is that there exists a complementary relation between the variance of H and the precision of θ estimation, quantified by the quantum Fisher information (QFI) [35–40]. This complementary relation can be regarded as not only a metrological steering inequality, but also a generalized local uncertainty relation.

The metrological steering task has so far been only investigated under a noiseless scenario, where the phase shift is generated by a perfect unitary evolution. However, in a real experimental setup, effects of noise are ubiquitous, such that the phase shifts could deviate from a perfect unitary and thus, neutralize quantum advantages in metrology [41–44]. A typical source of noise comes from the inevitable interaction between a given system and its uncontrollable environments. A question arises on how to mitigate the effects of these undesired interactions [45, 46]. Such a question has been addressed by applying many different methods, e.g., engineered reservoirs [47], measurement-error mitigation [45, 48] and dynamical decoupling [49].

Recently, a novel approach, termed *superposed quantum channels*, has been used to enhance quantum capacity in communication tasks [50–54]. In this framework, multiple quantum channels can be used. Furthermore, an additional quantum control was introduced to determine which channel for the target system to pass through; and hence, when the control system is prepared in a superposition state, the target system can go through these channels in a quantum superposition. In this sense, a superposition of noisy channels induces interference between alternative noisy processes. One can take advantage of this interference to alleviate the effects of noise via a suitable post-selection [55–57].

In this work, we consider the cases where the phase shifts are distorted by either pure dephasing noise or depolarizing noise. In this sense, we denote the corresponding noise-distorted phase shifts as dephased phase shifts and depolarized phase shifts, respectively. Intuitively, the violations of the metrological steering inequality decrease when the noise strengths increase in both cases. Further, we investigate the influences of post-selection

on the control system to the superposition of noisy phase shifts in the metrological steering task. We observe that for both types of superposed noisy phase shifts, the violations can be enhanced under a post-selection process. In addition, for the case of a superposition of depolarized phase shifts, we show that post-selection is able to delay the sudden-vanishing of the violation. Finally, we experimentally implement the metrological steering task with a superposition of dephased phase shifts on a IBM Quantum (IBM Q) computer [58–61]. We clearly observed the enhancement due to the post-selection of the outcome. We also provide noise simulations that take the inherent errors within the IBM Q device into account. Our experimental results agree with the corresponding noise simulations.

The rest of this work is organized as follows. In Sec. II, we review the metrological steering task proposed in Ref. [28] and extend the discussions to a scenario with superposition of noisy phase shifts. In Sec. III, we formalize the concept of superposition of noisy phase shifts and show that the post-selection technique can be used to mitigate the effects of noise. In Sec. IV, we show our experimental results obtained on a IBM Quantum computer. Finally, we summarize our results in Sec. V.

II. A METROLOGICAL STEERING TASK

In this section, we briefly recall the steering-enhanced quantum metrology proposed in Ref. [28]. We then extend the discussion to a scenario with superposition of dephased (depolarized) phase shifts.

We start by formulating the noiseless metrological task that a phase shift θ is generated by a unitary $\exp(-iH\theta)$, where H is the "generating" Hamiltonian. We consider a bipartite state ρ_{AB} shared between Alice and Bob. In each round of the experiment, Alice performs a measurement labelled by A. The probability to obtain the result a is denoted as $p(a|A)$; and the conditional reduced state of Bob's subsystem is $\rho_{B,a|A}$. After generating a local phase shift θ, Bob's conditional reduced state becomes $\rho_{B,a|A}(\theta) = \exp(-iH\theta)\rho_{B,a|A}\exp(iH\theta)$. It is convenient to summarize the result by defining an assemblage as a set of (subnormalized) quantum states, namely: $\{\mathcal{B}_\theta(a,A) = p(a|A)\rho_{B,a|A}(\theta)\}_{a,A,\theta}$.

After the measurement, Alice sends the classical information (a,A) to Bob. Based on this information, Bob can either measure the observable H or estimate the phase shift θ by measuring an observable M. Note that for a given message (a,A) from Alice, Bob can freely choose the observable M to obtain the maximum sensitivity, quantified by the QFI $F_Q\left(\theta|\rho_{B,a|A}\right)$ [41, 43, 62]. Here, $F_Q\left(\theta|\rho\right) := \mathrm{Tr}\left[L_\theta^2\rho(\theta)\right]$, where L_θ is the symmetric logarithmic derivate satisfying $\partial_\theta\rho(\theta) = \frac{1}{2}\{L_\theta,\rho(\theta)\}$ [31]. The optimal QFI and the optimal variance of H can be
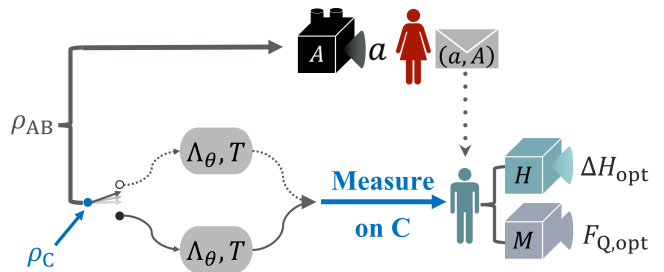

FIG. 1. Illustration of steering-enhanced quantum metrology with a superposition of quantum channels. Alice (A) and Bob (B) share a bipartite state ρ_{AB}. Alice performs a measurement A and obtains the corresponding outcome a. Then, Alice sends her information (a,A) to Bob through a classical communication. A local phase shift θ on Bob's side is generated by a Hamiltonian H. Different from Ref. [28], in which a phase shift is generated noiseless, we use a system C to control the evolution of system B and create a superposition of noisy phase shifts. When C is in the state $|0\rangle$ ($|1\rangle$), represented by the white (black) dot on the left, the system B interacts with the environment E_1 (E_2). After creating the superposition of noisy phase shifts, we collect the conditional state and measure on C. According to Alice's information, Bob can decide to either measure H or estimate the phase shift θ through the measurement M. Then, he can obtain the optimal variance ΔH_{opt} and QFI $F_{\mathrm{Q,opt}}$.

defined, respectively, as [28];

$$F_{\mathrm{Q,opt}} := \max_A \sum_a p(a|A)F_Q\left(\theta|\rho_{B,a|A}\right), \qquad (1)$$

$$\Delta H_{\mathrm{opt}} := \min_A \sum_a p(a|A)\Delta\left[\rho_{B,a|A}(\theta),H\right], \qquad (2)$$

where $\Delta[\rho,H] = \mathrm{Tr}\left[H^2\rho\right] - \mathrm{Tr}\left[H\rho\right]^2$. Note that, in general, the QFI is evaluated for a given θ [63].

In modern terminology, the concept of local-hidden-state (LHS) model is utilized to determine whether a given assemblage is steeerable or not. More specifically, an assemblage that admits a LHS model can be described as [2]

$$\mathcal{B}_\theta^{\mathrm{LHS}}(a,A) = \sum_\lambda p(\lambda)p(a|A,\lambda)\rho_{B,\lambda}(\theta) \quad \forall a,A, \qquad (3)$$

where $\{\rho_{B,\lambda}(\theta)\}_{\lambda,\theta}$ are quantum states and $\{p(a|A,\lambda)\}_\lambda$ constitute a stochastic map, which maps the hidden variable λ into $a|A$. If a given assemblage can be simulated by a LHS model, it is unsteerable. Otherwise, it is steerable. As reported in Ref. [28], when an assemblage is unsteerable, the metrological steering inequality (MSI) can be derived as $F_{\mathrm{Q,opt}} \leq 4\Delta H_{\mathrm{opt}}$. Here, we define the violation V of the MSI, i.e.,

$$V := \max\left(F_{\mathrm{Q,opt}} - 4\Delta H_{\mathrm{opt}}, 0\right). \qquad (4)$$

Therefore, $V > 0$ implies that the assemblage is steerable.

A	σ_x		σ_z	
a	0	1	0	1
$p(a\|A)$	0.5	0.5	0.5	0.5
$\rho_{a\|A}$	$\|+\rangle\langle+\|$	$\|-\rangle\langle-\|$	$\|0\rangle\langle0\|$	$\|1\rangle\langle1\|$

TABLE I. Summary of the results for Alice's measurements A with outcomes a, which include the probability $p(a|A)$ and the corresponding post-measurement state $\rho_{a|A}$.

III. A SUPERPOSITION OF NOISY PHASE SHIFTS

Throughout this work, we consider that a noisy phase shift can be described by a noiseless one followed by a noisy channel Λ [42], i.e.,

$$\Lambda_\theta(\rho) = \Lambda\left(e^{-iH\theta}\ \rho\ e^{iH\theta}\right). \tag{5}$$

We now consider a scenario for superposing two identical noisy phase shifts, as shown in Fig. 1. Recall that, as given in Eq. (5), a noisy phase shift (or any quantum process) can be effectively modeled as a quantum channel. According to Ref. [51], a superposition of multiple channels is well-defined if the implementation of each member channel is specified. More specifically, according to the Stinespring dilation theorem [64–66], there exist non-unique system-environment models to describe a quantum channel Λ_θ, namely

$$\exists U_{\mathrm{BE}},\ \mathcal{E}_{\mathrm{E}}\ \text{s.t}\ \Lambda_\theta(\rho) = \mathrm{Tr}_{\mathrm{E}}[U_{\mathrm{BE}}(\rho\otimes\mathcal{E}_{\mathrm{E}})U_{\mathrm{BE}}^\dagger)], \tag{6}$$

where U_{BE} denotes the system-environment global unitary, and $\mathcal{E}_{\mathrm{E}}$ is an initial state of the environment. The superposition of two identical channels Λ_θ for a given implementation can be described by

$$U_{\mathrm{tot}} = |0\rangle\langle0|_{\mathrm{C}}\otimes\ U_{\mathrm{BE}_1} + |1\rangle\langle1|_{\mathrm{C}}\otimes\ U_{\mathrm{BE}_2}. \tag{7}$$

Here, we introduce a quantum control C to determine which environment (i.e., E_1 or E_2,) affects the system B. If the total system is initially prepared in

$$\rho_{\mathrm{tot}} = |j\rangle\langle j|_{\mathrm{C}}\otimes\rho\otimes\mathcal{E}_{\mathrm{E}_1}\otimes\mathcal{E}_{\mathrm{E}_2} \tag{8}$$

for j being either 0 or 1, the reduced state of C and B reads

$$\begin{aligned}
\rho_{\mathrm{CB}}(\theta) &= \mathrm{Tr}_{\mathrm{E}_1,\mathrm{E}_2}\left[U_{\mathrm{tot}}\left(|j\rangle\langle j|_{\mathrm{C}}\otimes\rho\otimes\mathcal{E}_{\mathrm{E}_1}\otimes\mathcal{E}_{\mathrm{E}_2}\right)U_{\mathrm{tot}}^\dagger\right]\\
&= |j\rangle\langle j|_{\mathrm{C}}\otimes\mathrm{Tr}_{\mathrm{E}_j}[U_{\mathrm{BE}_j}(\rho\otimes\mathcal{E}_{\mathrm{E}_j})U_{\mathrm{BE}_j}^\dagger]\\
&= |j\rangle\langle j|_{\mathrm{C}}\otimes\Lambda_\theta(\rho).
\end{aligned} \tag{9}$$

In other words, when C is prepared in the state $|j\rangle$, B interacts with the corresponding environment E_j.

On the other hand, if the quantum control C is prepared in a superposition state $|\alpha\rangle = \sqrt{\alpha}|0\rangle + \sqrt{1-\alpha}|1\rangle$, with $0 \le \alpha \le 1$, we obtain

$$\begin{aligned}
\rho_{\mathrm{CB}}(\theta) = &[\ \alpha|0\rangle\langle0|_{\mathrm{C}} + (1-\alpha)|1\rangle\langle1|_{\mathrm{C}}\ ]\otimes\Lambda_\theta(\rho)\\
&+ \sqrt{\alpha(1-\alpha)}(|0\rangle\langle1|_{\mathrm{C}} + |1\rangle\langle0|_{\mathrm{C}})\otimes T\rho\, T^\dagger,
\end{aligned} \tag{10}$$

where $T = \mathrm{Tr}_{\mathrm{E}}\left(U_{\mathrm{BE}}\ \rho\otimes\mathcal{E}\right)$ characterizes the quantum interference effects between these two channels [51]. Note that we have omitted the subscripts for the environments because they are isomorphic to each other. Now, we perform a set of projective measurements, $\{|+\rangle\langle+|,|-\rangle\langle-|\}$ with $|\pm\rangle = (|0\rangle\pm|1\rangle)/\sqrt{2}$, on the quantum control C. The conditional states of B then read

$$\begin{aligned}
\rho_{B,\pm}(\theta) &= \frac{\mathrm{Tr}_{\mathrm{C}}\left[(|\pm\rangle\langle\pm|_{\mathrm{C}}\otimes\mathbb{1}_{\mathrm{B}})\ \rho_{\mathrm{CB}}(\theta)\right]}{\mathrm{Tr}\left[(|\pm\rangle\langle\pm|_{\mathrm{C}}\otimes\mathbb{1}_{\mathrm{B}})\ \rho_{\mathrm{CB}}(\theta)\right]}\\
&= \frac{\Lambda_\theta(\rho)}{2P_\pm} \pm \frac{\sqrt{\alpha(1-\alpha)}}{P_\pm}T\rho\,T^\dagger,
\end{aligned} \tag{11}$$

where $P_\pm = \mathrm{Tr}\left[(|\pm\rangle\langle\pm|_{\mathrm{C}}\otimes\mathbb{1}_{\mathrm{B}})\ \rho_{\mathrm{CB}}(\theta)\right]$ are the successful probabilities of the outcomes $\pm$ for the projective measurements. Equation (11) shows that the post-measurement state does not only depend on the noisy phase shift Λ_θ, but also depends on the quantum interference effects described by T.

We are now ready to demonstrate the main result of this work, i.e., the superposition of phase shifts can enhance the violations of the MSI. We consider the unitaries U_w^{deph} and U_v^{depo}, with visibilities w and v, to implement the dephased and depolarized phase shifts, respectively, i.e.,

$$\begin{aligned}
U_w^{\mathrm{deph}}|\psi\rangle\otimes|0\rangle_{\mathrm{E}} = &\sqrt{1-\frac{w}{2}}\ |\psi_\theta\rangle\otimes|0\rangle_{\mathrm{E}}\\
&+ \sqrt{\frac{w}{2}}\ \sigma_z|\psi_\theta\rangle\otimes|1\rangle_{\mathrm{E}},
\end{aligned} \tag{12}$$

$$\begin{aligned}
U_v^{\mathrm{depo}}|\psi\rangle\otimes|0\rangle_{\mathrm{E}} = &\sqrt{1-\frac{3v}{4}}|\psi_\theta\rangle\otimes|0\rangle_{\mathrm{E}}\\
&+ \sqrt{\frac{v}{4}}\sigma_x|\psi_\theta\rangle\otimes|1\rangle_{\mathrm{E}}\\
&+ \sqrt{\frac{v}{4}}\sigma_y|\psi_\theta\rangle\otimes|2\rangle_{\mathrm{E}}\\
&+ \sqrt{\frac{v}{4}}\sigma_z|\psi_\theta\rangle\otimes|3\rangle_{\mathrm{E}},
\end{aligned} \tag{13}$$

where $|\psi_\theta\rangle = \exp(-iZ\theta)|\psi\rangle$.

According to Eq. (11), the states conditioned on the result "+" can then be written as

$$\begin{aligned}
\rho_{\mathrm{B},a|A,+}^{\mathrm{deph}}(\theta) &= \frac{\Lambda_{\theta,w}^{\mathrm{deph}}(\rho_{\mathrm{B},a|A}) + (1-\frac{w}{2})e^{-iZ\theta}\rho_{\mathrm{B},a|A}e^{iZ\theta}}{2-\frac{w}{2}},\\
\rho_{\mathrm{B},a|A,+}^{\mathrm{depo}}(\theta) &= \frac{\Lambda_{\theta,v}^{\mathrm{depo}}(\rho_{\mathrm{B},a|A}) + \left(1-\frac{3v}{4}\right)e^{-iZ\theta}\rho_{\mathrm{B},a|A}e^{iZ\theta}}{2-\frac{3v}{4}}.
\end{aligned} \tag{14}$$

One can find that, for both cases, the results of the post-selection can be effectively characterized by a mixture of a noisy phase shift and a noiseless one, implying that the effects of noise can be probabilistically decreased. However, if we do not select the result, we obtain the state corresponding to a direct trace-out of the dimension of C

in Eq. (10). Therefore, the reduced state only depends on a single-use of the noisy phase shift, i.e., $\rho_B = \Lambda_\theta(\rho)$. In Fig. 2, we present the violations for the cases; (1) a superposition of dephased (depolarized) phase shifts without selecting the result on C as V_w^{deph} (V_v^{depo}) and (2) with post-selection on the result "+", i.e., $\tilde{V}_w^{\text{deph}}$ ($\tilde{V}_v^{\text{depo}}$). For the case with the superposition of pure dephased phase shifts, as shown in Fig. 2(a), one can observe that post-select the results on C has a clear enhancement on the violations for a given visibility w. Although the system is completely dephased, we still can find the violation ≈ 0.11. In addition, without a post-selection of the depolarized one, as shown in Fig. 2(b), the sudden-vanishing of the violation occurs when $v \approx 0.29$, while post-select the result on "+" extends the effect to $v \approx 0.48$.
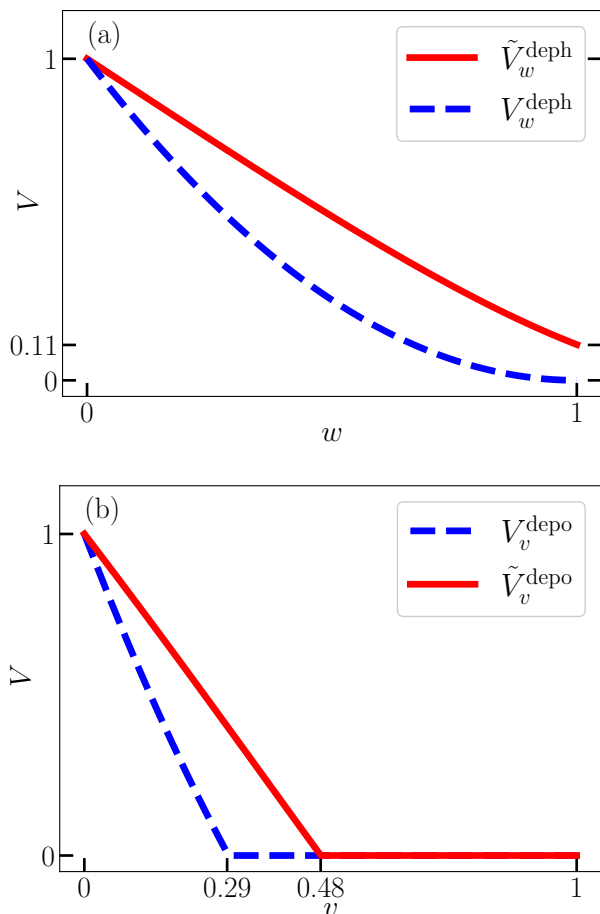
FIG. 2. Violations of the metrological steering inequality for the case with a superposition of (a) pure dephased and (b) depolarized phase shifts. We take $\theta = 0$ and plot the violations in Eq. (4) with respect to the visibilities w and v. One can observe the enhancement due to the post-selection on the result for a given visibility. Additionally, for the case of dephased phase shift (a), we can observe that although the system is fully dephased, we still can witness the violation ≈ 0.11 in the post-selection case. Also, for the case with depolarized phase shift (b), the sudden-vanishing effect of the violation can be extended from $v \approx 0.29$ to $v \approx 0.48$.

IV. EXPERIMENTAL DEMONSTRATION

In this section, we propose a circuit model of superposition of dephased phase shift that only consists of 12 CNOT gates and 17 single-qubit gates, and demonstrate the enhancement on a IBM Q processor. Additionally, we use a model to simulate the device-intrinsic noise to identity the effects of noise in our experimental data.

To further decrease the circuit depth, we consider a scenario known as temporal quantum steering [67–69]. Therein, the initial maximally entangled state shared by Alice and Bob can be replaced by a prepare-and-measure scenario [70–72]. More specifically, instead of performing local measurements on the bipartite state $|\psi_{\text{AB}}\rangle$, Alice now measures σ_x and σ_z on a maximally mixed state $\mathbb{1}/2$. Then, the probability $p(a|A)$ and the post-measurement state $\rho_{a|A}$ are exactly the same as those in Table I. Since the IBM Q does not allow us to obtain the post-measurement state, we directly prepare the eigenstates of σ_x and σ_z. Further, we assume that $p(a|A) = 1/2 \ \forall a, A$.

A. Circuit implementation on the IBM Q

As shown in Fig. 3, we provide a circuit model to experimentally implement the metrological steering task with the superposition of dephased phase shifts described in the previous section [Eqs. (7) and (12)]. This circuit involves four qubits, which serve as the control C, the system B, and the two environments, E_1 and E_2, respectively. Because CNOT gates on the IBM Q are restricted by the connectivity of the devices, we find that the implementation of the circuit on the devices with the coupling map shown in Fig. 3(b) can minimize the number of CNOT gates.

This circuit can be divided into three parts: (i) state preparation, (ii) the superposition of dephased phase shifts, and (iii) measurement on the qubits C and B. In part (i), the qubits C, B, and $E_{1,(2)}$ are prepared in the states $|+\rangle \langle+|$, $\rho_{a|A}$, and $|0\rangle \langle0|_{1,(2)}$, respectively. In the IBM Q device, all qubits are initially in state $|0\rangle$. The state preparation can be achieved by applying single-qubit gates on each qubit. For instance, we can obtain a $|+\rangle_C$ by applying a Hadamard gate on the control system C.

In part (ii), the circuit model of the superposition of dephased-noise phase shifts is shown in Fig. 3(a). The qubit topology of the four qubits that we chose in IBM-Cairo is shown in Fig. 3(b). Through the control qubit C, the system B can interact with alternative environments. We divide the total unitary in Fig. 3(a) into a gate sequence which is shown in Fig. 3(c). In this sequence, we use control-rotation with angle ϕ on the system B and its respective environment. After we trace out its environment, this control-rotation gate is effectively equal to the pure dephasing noise on the system B. Here, the visibility of the pure dephasing noise w is tuned by the angle ϕ, such that $\phi = 2\sin^{-1}(\sqrt{w/2})$, with $\phi \in [0, \pi/2]$. In part
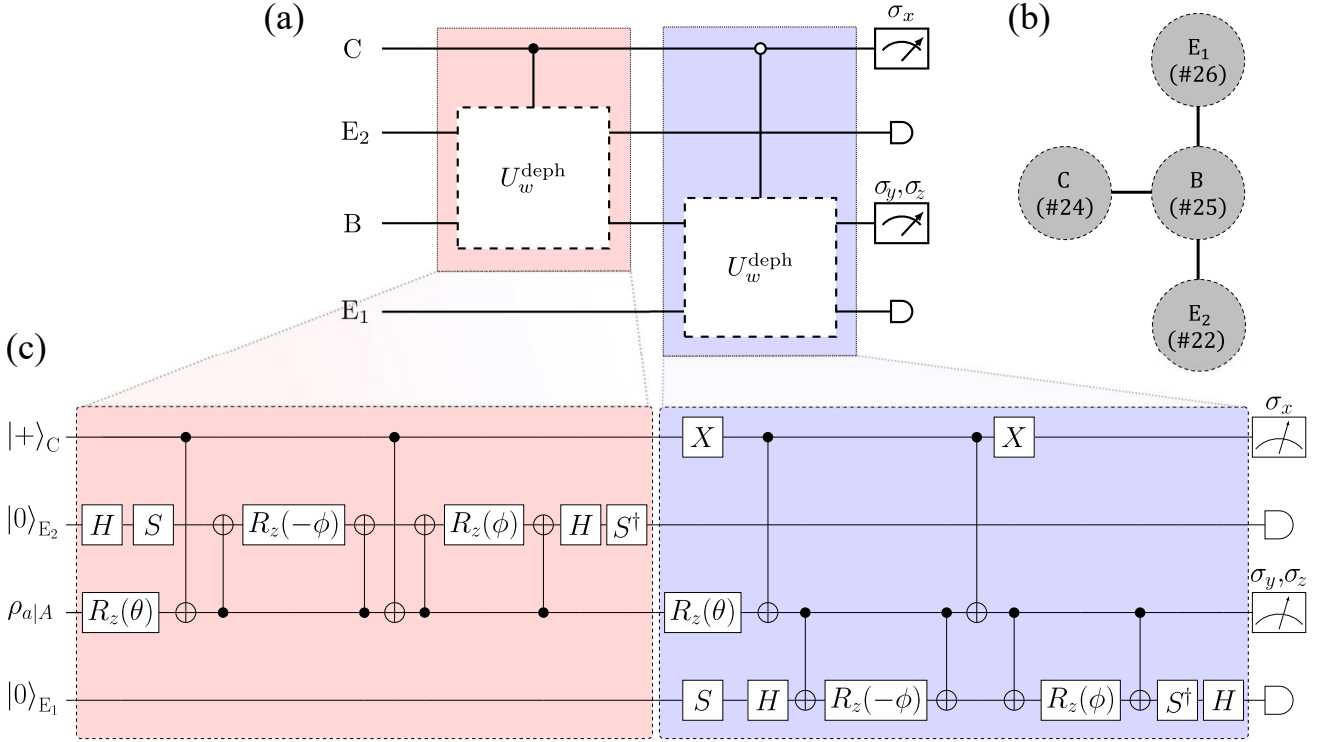
FIG. 3. Circuit model for steering-enhanced quantum metrology with a superposition of noisy phase shifts. Schematics: (a) circuit model without and (c) with details. (b) In the topology of the four qubits we chose in the IBM-Cairo device device, the numbers are the labels of the qubits #24, #25, #26, #22, representing the system C, B, E_1, E_2, respectively. Here, the visibility w is tuned by the angle ϕ such that $w = 2\sin^2(\phi/2)$. We use the standard symbols for quantum gates (see Appendix A).

(iii), we measure σ_x on qubit C and measure σ_z or σ_y on qubit B. Note that IBM Q only allow us to conduct measurement σ_z, therefore, we can apply a Hadamard gate (H) on the qubit before the IBM Q-measure to measure σ_x, and a phase gate (S) plus Hadamard gate to obtain the measurement σ_y.

Let us now elaborate how to obtain the Fisher information (FI) and the variance from the measurement results. The measurement data can be summarized by a set of probabilities $\{p_{\theta,\phi}(b,c|M,\rho_{a|A})\}$, where $M \in \{\sigma_z, \sigma_y\}$ denotes Bob's measurement with the outcome $b \in \{0,1\}$, and $c \in \{0,1\}$ is the outcome of measuring σ_x on C. Note that $\{M_b\}_b$ is the set of positive operators that satisfy $\sum_b M_b = \mathbb{1}$. The probability $p(b|M)$ is given by the Born rule, that is, $p(b|M) = \text{Tr}[M_b\rho]$. As aforementioned, we can decide whether to select the outcome $c = 0$ associated with the eigenstate $|+\rangle_\text{C}$. However, if we take both the outcomes $c = 0$ and $c = 1$ into account, we obtain the result without post-selection. The marginal probabilities then reads

$$p_{\theta,\phi}(b|M,\rho_{a|A}) = \sum_c p_{\theta,\phi}(b,c|M,\rho_{a|A}). \quad (15)$$

For the case of post-select the result on $|+\rangle_\text{C}$, we fix $c = 0$

to obtain the probability

$$p_{\theta,\phi}(b|M,c=0,\rho_{a|A}) = \frac{p_{\theta,\phi}(b,c=0|M,\rho_{a|A})}{\sum_b p_{\theta,\phi}(b,c=0|M,\rho_{a|A})}. \quad (16)$$

We can then obtain the optimal variance ΔH_opt by Eq. (2).

In addition, the optimal FI can be expressed as

$$F_\text{opt} := \max_A \sum_a p(a|A)F\left(\theta|M,\rho_{a|A}\right). \quad (17)$$

Here, $F\left(\theta|M,\rho_{a|A}\right)$ denotes the FI of a conditional state $\rho_{a|A}$, which is defined as

$$F\left(\theta|M,\rho_{a|A}\right) := \sum_b \frac{\left[\partial_\theta p_\theta(b|M,\rho_{a|A})\right]^2}{p_\theta(b|M,\rho_{a|A})}. \quad (18)$$

Note that the FI for a given measurement M is a lower bound of QFI i.e., $F\left(\theta|M,\rho_{a|A}\right) \leq F_\text{Q}(\theta|\rho_{a|A})$ [31], and thus, $F_\text{opt} \leq F_\text{Q,opt}$.

We implement our proposal on IBM-Cairo device because it has longer relaxation and coherence times, i.e., T_1, T_2, and lower gate errors than other available IBM Q devices (see Table. II and the information from IBM Q website [73]). In addition, we choose the qubits, labeled by #25, #24, #26, and #22 in the device, to represent
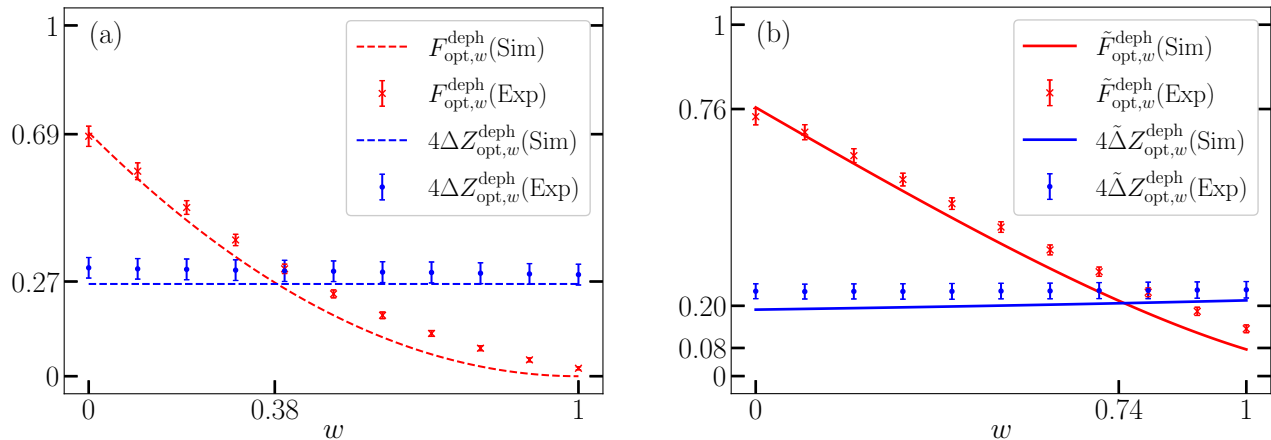
FIG. 4. Experimental results and noisy simulations of: (a) Superposition of dephased phase shifts *without* post-selection, and (b) Superposition of dephased phase shifts *with* post-selection. The red-x (blue-circle) data points are the experimental results of optimal Fisher information (optimal variance) with respect to the visibility w of superposition of dephased phase shifts. Here, the error bars are calculated by 40 rounds of experiments and we choose $\theta = 0$. The solid curves represent the noisy simulations for the post-selected outcome "+" on the control system C; the dashed curves represent the noisy simulations without post-selection. Our experimental results agree with the noise simulations in both cases (a) and (b). We observe that by post-selecting the outcome "+" on the control system C can clearly enhance the optimal Fisher information and decrease the optimal variation; and thus, enhance the violations of the metrological steering inequality from $w \approx 0.38$ to $w \approx 0.74$.

B, C, E_1, and E_2, respectively because of their connectivities [see Fig. 3(b)]. As shown in Fig. 4, we provide the results by conducting experiments on the IBM-Cairo device with $10,000$ shots for each data point.

To calculate the partial derivative of the probability in Eq. (18), we use a fitting function $g(\theta) = 0.5 + \alpha \sin(2\theta + \beta)$ to interpolate the $p_{\theta,\phi}$, where α and β are fitting parameters. Also, we take $\theta = 0$ to obtain the maximum value of the optimal FI. We observe that the superposition can increase F_{opt} and decrease ΔZ_{opt}. The threshold of the MSI violations can be increased by post-selection, i.e., from $w \approx 0.38$ to $w \approx 0.74$.
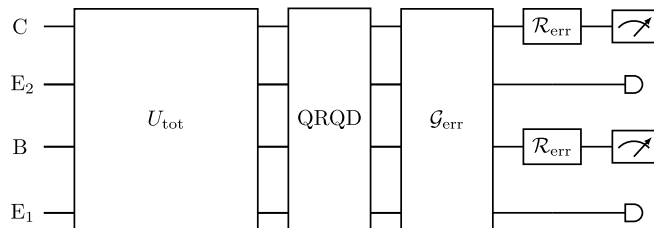

FIG. 5. The model of noisy simulations. We model the qubit relaxation and qubit dephasing effect that occurs after performing a total unitary evolution. After that, we apply depolarizing channels to describe gate errors and bit-flip channels both on B and C to simulate the readout errors.

B. Noise simulations

Here, we also provide noise simulations by using NumPy and QuTip [74–76] (see also the similar discus-

sion in Ref. [77, 78]). In our noise model, we consider three different sources of the intrinsic noise from the device: qubit relaxation and qubit dephasing (QRQD), CNOT error, and readout error.

First, the QRQD is modeled by the following Lindblad master equation [79]:

$$\frac{\partial \rho(t)}{\partial t} = \sum_{m}^{n} \frac{\gamma_{T_1}^{(m)}}{2} \left[2\sigma_-^{(m)} \rho(t) \sigma_+^{(m)} - \{\sigma_-^{(m)}\sigma_+^{(m)}, \rho(t)\} \right]$$
$$+ \sum_{m}^{n} \frac{\gamma_{T_2}^{(m)}}{2} \left[2\sigma_z^{(m)} \rho(t) \sigma_z^{(m)} - \{\sigma_z^{(m)2}, \rho(t)\} \right], \tag{19}$$

where $\gamma_{T_1}^{(m)} = 1/T_1^{(m)}$ and $\gamma_{T_2}^{(m)} = 1/T_1^{(m)} - 1/(2T_2^{(m)})$ are the mth qubit relaxation and decoherence rates, respectively. Here, $\sigma_+(\sigma_-)$ denotes the atomic creation (annihilation) operator, and the corresponding relaxation (dephasing) time T_1 (T_2) are summarized in Table II. We model the QRQD effect that occurs after performing a total unitary evolution (see Fig. 5) and simulate it using the master equation solver MESOLVE in QuTip. We sum over all the gate times in the circuit and obtain the total gate time $\approx 3,725$ ns. Note that each Pauli X gate in IBM-Cairo device takes 21.3 ns, and the Hadamard gate H (phase gate S) gate takes 5 (3) times longer than that of the Pauli X gate, respectively.

Second, the gate error is determined from the randomized benchmarking [80, 81]. In a quantum assembly simulator, the gate error for the n-qubits system can be modeled by depolarizing noise [82], i.e.,

$$\mathcal{G}_{\mathrm{err}}(\rho) = (1 - \Gamma_{\mathrm{G}})\rho + \Gamma_{\mathrm{G}}\frac{\mathbb{1}}{2^n}, \tag{20}$$

Qubits	T_1 (μs)	T_2 (μs)	Γ_X (10^{-4})	Γ_{R} (10^{-2})
B	118.4	194.5	1.5	1.0
C	122.2	196.5	4.7	1.5
E_1	84.1	44.1	1.7	0.1
E_2	102.3	138.4	3.0	2.1

CNOT gate	CNOT error (10^{-3})	Gate time (ns)
B $-$ C	6.8	309.3
B $-$ E_1	6.6	248.9
B $-$ E_2	9.0	202.7

TABLE II. Error parameters in the IBM-Cairo device. The number of the four qubits in IBM-Cairo device are labeled as: #25, #24, #26, and #22, representing the systems B, C, E_1, and E_2, respectively. Where T_1 (T_2) is the relaxation (dephasing) time, Γ_X is the Pauli gate error, and Γ_R is the readout error. Note that these error rates are public information on the IBM Q website [73]. These numbers are presented here for completeness.

where Γ_{G} is the gate error rate. In our model, we assume that the gate errors are sequentially accumulated; thus, we multiply the different error rates which appear in the circuit. Inserting the CNOT-gates error rate and the single-qubit Pauli-gates error rate Γ_X shown in Table. II, we obtain this gate error rate effect to about 9.2%.

Finally, the readout error occurs because quantum devices have the probability of misrecording the ideal result $0(1)$ as $1(0)$, respectively. Therefore, it can be modeled by a bit-flip channel, i.e.,

$$\mathcal{R}_{\mathrm{err}}(\rho) = (1 - \Gamma_{\mathrm{R}})\rho + \Gamma_{\mathrm{R}}\ \sigma_x \rho \sigma_x, \qquad (21)$$

where Γ_{R} is the probability of the readout error.

As a result, the primary source causing errors is the number of CNOT gates, because they create a significant error rate compared to single-qubit gates. Moreover, the CNOT-gates also take longer time [76], meaning that they also increase the error effects from the QRQD. Although we have "only" used 12 CNOT-gates and 17 single-qubit gates in our circuit implementation of a superposition of the dephased phase shifts, it still creates errors greater than 21.6% *with* post-selection and 27.0% *without* post-selection. For the depolarized phased shift, the used Toffoli gates implemented by numerous CNOT-gates, we find that the number of CNOT gates needed is ≥ 328. With this number of CNOT gates, the circuit depth and gate errors can destroy any kind of quantum advantages, which we discuss in Appendix A.

V. SUMMARY

In this work, we generalized the metrological steering task described in Ref. [28] to a scenario with noisy phase shifts. We show that the violations of the MSI, given in Eq. (4), monotonically decreases for the superposition of dephased or depolarized phase shifts. Further, we show that by post-select the outcome "+" on the control system, we can enhance the violations of the MSI in comparison with the case without the post-selection.

Moreover, we proposed a circuit model for superposing two dephased phase shifts and experimentally implemented the circuit on IBM Quantum computer. We clearly observe the violations of the MSI, and the experimental results agree with our noise simulations.

Finally, it is known that the order of channels can also be coherently controlled [83, 84]. Therefore, it would be promising to apply this framework to the noisy metrological steering task.

ACKNOWLEDGMENTS

Appendix A: Circuit model of a superposition of depolarized phase shifts

In this Appendix, we aim to construct a circuit that satisfies the depolarized phase shifts implementing the
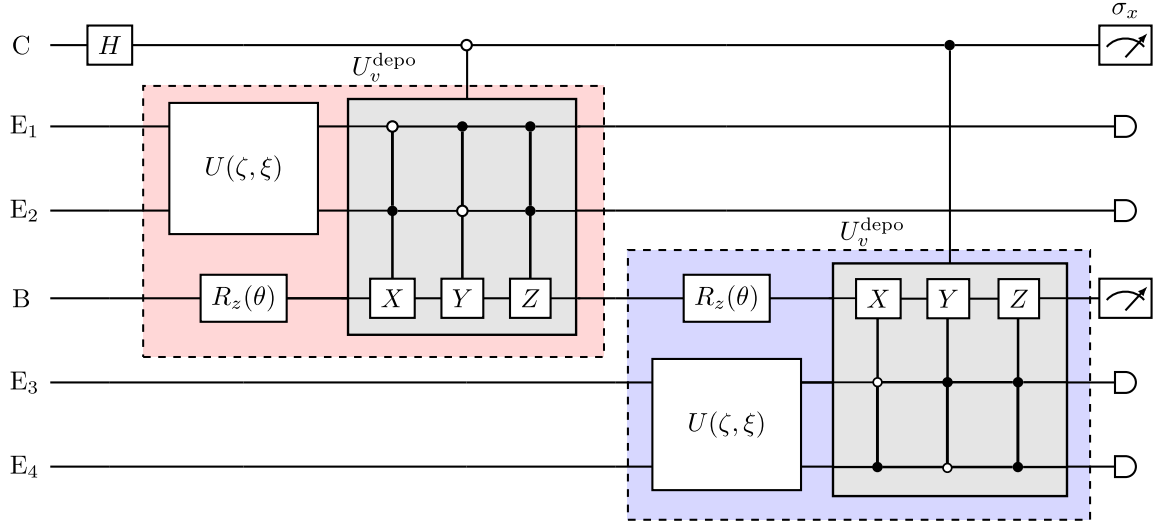
FIG. 6. Circuit implementing a superposition of depolarized phase shifts. We assume that all the environments E and control C are initialized to $|0\rangle$.

operations in Eq. (13). A direct way to design a depolarizing phase shift circuit is that we can use three different kinds of Toffoli gates to represent the system transformation errors modeled by σ_x, σ_y, and σ_z with different probabilities [86]. As shown in Fig. 6, we use a two-qubit system, which plays a role of a four-level environment in Eq. (13), i.e.,

$$
\begin{aligned}
|0\rangle_{\mathrm{E}} &\to |0\rangle |0\rangle_{\mathrm{E}}, & |1\rangle_{\mathrm{E}} &\to |0\rangle |1\rangle_{\mathrm{E}}, \\
|2\rangle_{\mathrm{E}} &\to |1\rangle |0\rangle_{\mathrm{E}}, & |3\rangle_{\mathrm{E}} &\to |1\rangle |1\rangle_{\mathrm{E}}.
\end{aligned} \tag{A1}
$$

To fit the factors $\sqrt{1 - \frac{3v}{4}}$ and $\sqrt{\frac{v}{4}}$ in Eq. (13), we apply
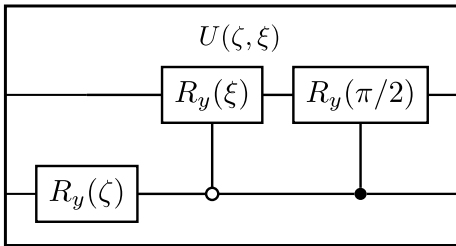

FIG. 7. Circuit implementing the unitary operation $U(\zeta, \xi)$, which maps $|0\rangle |0\rangle_{\mathrm{E}}$ onto the state in (A3).

a unitary $U(\zeta, \xi)$, which maps the two-qubit environment $|0\rangle |0\rangle_{\mathrm{E}}$ into

$$
\sqrt{1 - 3v/4}\, |0\rangle |0\rangle_{\mathrm{E}} + \sqrt{v/4}\left(|0\rangle |1\rangle_{\mathrm{E}} + |1\rangle |0\rangle_{\mathrm{E}} + |1\rangle |1\rangle_{\mathrm{E}} \right) \tag{A2}
$$

with two rotation parameters ζ and ξ on the environmental system (see also Fig. 7). After mapping $U(\zeta, \xi)$, we

obtain the initial state

$$
\begin{aligned}
|0\rangle |0\rangle_{\mathrm{E}} \to &\cos\frac{\zeta}{2}\cos\frac{\xi}{2} |0\rangle |0\rangle_{\mathrm{E}} + \sqrt{\frac{1}{2}}\sin\frac{\zeta}{2} |0\rangle |1\rangle_{\mathrm{E}} \\
&+ \cos\frac{\zeta}{2}\sin\frac{\xi}{2} |1\rangle |0\rangle_{\mathrm{E}} + \sqrt{\frac{1}{2}}\sin\frac{\zeta}{2} |1\rangle |1\rangle_{\mathrm{E}}.
\end{aligned} \tag{A3}
$$

One can find that if we let $\zeta = 2\sin^{-1}\sqrt{v/2}$ and $\xi = 2\sin^{-1}\sqrt{v/(4 - 2v)}$, we can obtain the red (blue) box in Fig. 6, which is equal to U_v^{depo} in Eq. (13).

In general, to implement a superposition of quantum channels in a gate-based quantum simulation requires using many Toffoli gates [87, 88]. For the superposition of two depolarized phase shifts, we require an additional control system. Therefore, there are six controlled Toffoli gates required to simulate the desired dynamics (see Fig. 6). Since a Toffoli gate can be decomposed into six CNOT gates and nine single-qubit gates [86], therefore, a single controlled Toffoli gate contains 52 CNOT gates and needs $\approx 16{,}400$ ns to operate.

In total, there are 328 CNOT gates in our circuit, creating the gate-error rates of at least 94.3%, and a total gate time $\approx 111{,}945$ ns. The noise simulations of the depolarized noise phase shifts are shown in Fig. 8. We note that $4\tilde{\Delta}Z_{\mathrm{opt},v}^{\mathrm{depo}}$ is larger than 0.99 and the $\tilde{F}_{\mathrm{opt},v}^{\mathrm{depo}}$ is less than 0.01. Thus, we do not observe the violation of the metrological steering inequality in Eq. (4) on IBM Q devices since the circuits error is too large and destroys the quantum advantages.

For clarity and completeness, we recall the meaning of standard gates used in our implementation both in Fig. 3 and Fig. 6. Specifically, X, Y, Z, represent Pauli gates, H the Hadamard gate, and S the phase gate, defined as $S = \mathrm{diag}(1, i)$. Also, $R_z(\theta)$ is the rotation gate along the z-axis with angle θ, written as $R_z(\theta) = \mathrm{diag}[\exp{(-i\theta/2)}, \exp{(i\theta/2)}]$. The black-dot two-qubit
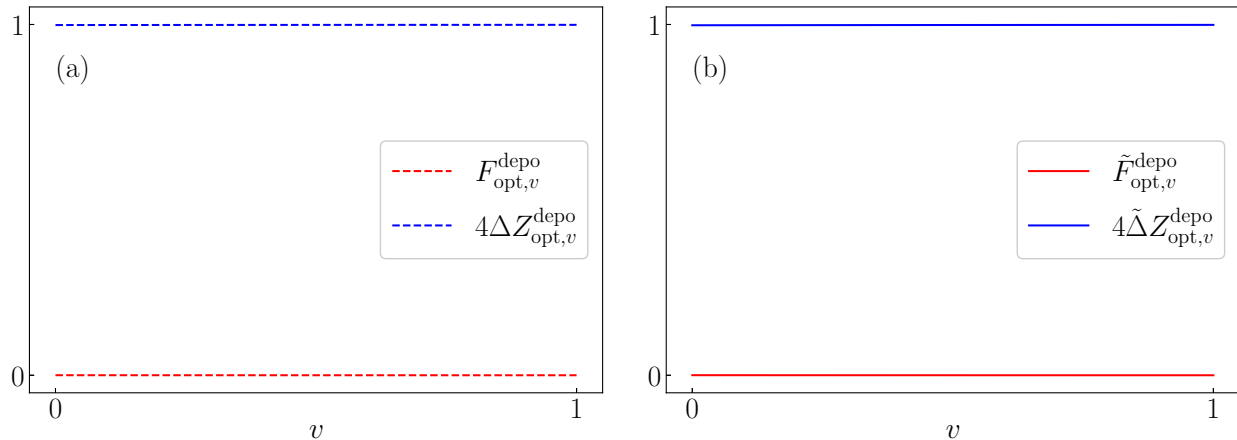
FIG. 8. Noise simulations of the superposition of depolarized phase shifts for: (a) *without* post-selection and (b) *with* post-selection. We find that both optimal Fisher information in (a) and (b) are less than 0.01 and both optimal variations are larger than 0.99, such that there is no violation of the metrological steering inequality for all visibility v.

gates in Fig. 3 are the controlled-NOT (CNOT) gates, while the three-qubit gates in Fig. 6 are different types of Toffoli gates, i.e., the double CNOT gates [86].

[1] E. Schrödinger, Probability relations between separated systems, Math. Proc. Cambridge **32**, 446 (1936).

[2] H. M. Wiseman, S. J. Jones, and A. C. Doherty, Steering, entanglement, nonlocality, and the Einstein-Podolsky-Rosen paradox, Phys. Rev. Lett. **98**, 140402 (2007).

[3] D. Cavalcanti and P. Skrzypczyk, Quantum steering: a review with focus on semidefinite programming, Rep. Prog. Phys. **80**, 024001 (2016).

[4] R. Uola, A. C. S. Costa, H. C. Nguyen, and O. Gühne, Quantum steering, Rev. Mod. Phys. **92**, 015001 (2020).

[5] D. J. Saunders, S. J. Jones, H. M. Wiseman, and G. J. Pryde, Experimental EPR-steering using Bell-local states, Nat. Phys. **6**, 845 (2010).

[6] A. J. Bennet, D. A. Evans, D. J. Saunders, C. Branciard, E. G. Cavalcanti, H. M. Wiseman, and G. J. Pryde, Arbitrarily loss-tolerant Einstein-Podolsky-Rosen steering allowing a demonstration over 1 km of optical fiber with no detection loophole, Phys. Rev. X **2**, 031003 (2012).

[7] C.-M. Li, K. Chen, Y.-N. Chen, Q. Zhang, Y.-A. Chen, and J.-W. Pan, Genuine high-order Einstein-Podolsky-Rosen steering, Phys. Rev. Lett. **115**, 010402 (2015).

[8] S. Wollmann, R. Uola, and A. C. S. Costa, Experimental demonstration of robust quantum steering, Phys. Rev. Lett. **125**, 020404 (2020).

[9] X. Deng, Y. Liu, M. Wang, X. Su, and K. Peng, Sudden death and revival of Gaussian Einstein–Podolsky–Rosen steering in noisy channels, npj Quantum Inf. **7**, 65 (2021).

[10] S. Slussarenko, D. J. Joch, N. Tischler, F. Ghafari, L. K. Shalm, V. B. Verma, S. W. Nam, and G. J. Pryde, Quantum steering with vector vortex photon states with the detection loophole closed, npj Quantum Inf. **8**, 20 (2022).

[11] M. T. Quintino, T. Vértesi, and N. Brunner, Joint mea-surability, Einstein-Podolsky-Rosen steering, and bell nonlocality, Phys. Rev. Lett. **113**, 160402 (2014).

[12] R. Uola, T. Moroder, and O. Gühne, Joint measurability of generalized measurements implies classicality, Phys. Rev. Lett. **113**, 160403 (2014).

[13] R. Uola, C. Budroni, O. Gühne, and J.-P. Pellonpää, One-to-one mapping between steering and joint measurability problems, Phys. Rev. Lett. **115**, 230402 (2015).

[14] D. Schmid, D. Rosset, and F. Buscemi, The type-independent resource theory of local operations and shared randomness, Quantum **4**, 262 (2020).

[15] S.-L. Chen, H.-Y. Ku, W. Zhou, J. Tura, and Y.-N. Chen, Robust self-testing of steerable quantum assemblages and its applications on device-independent quantum certification, Quantum **5**, 552 (2021).

[16] H.-Y. Ku, C.-Y. Hsieh, S.-L. Chen, Y.-N. Chen, and C. Budroni, Complete classification of steerability under local filters and its relation with measurement incompatibility, arXiv:2201.07691 (2022).

[17] M. Fadel and M. Gessner, Entanglement of Local Hidden States, Quantum **6**, 651 (2022).

[18] C. Branciard, E. G. Cavalcanti, S. P. Walborn, V. Scarani, and H. M. Wiseman, One-sided device-independent quantum key distribution: Security, feasibility, and the connection with steering, Phys. Rev. A **85**, 010301(R) (2012).

[19] M. Piani and J. Watrous, Necessary and sufficient quantum information characterization of Einstein-Podolsky-Rosen steering, Phys. Rev. Lett. **114**, 060404 (2015).

[20] D. Cavalcanti and P. Skrzypczyk, Quantitative relations between measurement incompatibility, quantum steering, and nonlocality, Phys. Rev. A **93**, 052112 (2016).

[21] Y.-Y. Zhao, H.-Y. Ku, S.-L. Chen, H.-B. Chen, F. Nori, G.-Y. Xiang, C.-F. Li, G.-C. Guo, and Y.-N.

Chen, Experimental demonstration of measurement-device-independent measure of quantum steering, npj Quantum Inf. **6**, 77 (2020).

[22] E. Y.-Z. Tan, R. Schwonnek, K. T. Goh, I. W. Primaatmaja, and C. C.-W. Lim, Computing secure key rates for quantum cryptography with untrusted devices, npj Quantum Inf. **7**, 158 (2021).

[23] J. Bohr Brask, F. Clivaz, G. Haack, and A. Tavakoli, Operational nonclassicality in minimal autonomous thermal machines, Quantum **6**, 672 (2022).

[24] H.-Y. Ku, J. Kadlec, A. Černoch, M. T. Quintino, W. Zhou, K. Lemr, N. Lambert, A. Miranowicz, S.-L. Chen, F. Nori, and Y.-N. Chen, Quantifying quantumness of channels without entanglement, PRX Quantum **3**, 020338 (2022).

[25] M. D. Reid, P. D. Drummond, W. P. Bowen, E. G. Cavalcanti, P. K. Lam, H. A. Bachor, U. L. Andersen, and G. Leuchs, Colloquium: The Einstein-Podolsky-Rosen paradox: From concepts to applications, Rev. Mod. Phys. **81**, 1727 (2009).

[26] E. G. Cavalcanti, S. J. Jones, H. M. Wiseman, and M. D. Reid, Experimental criteria for steering and the Einstein-Podolsky-Rosen paradox, Phys. Rev. A **80**, 032112 (2009).

[27] J. Dressel and F. Nori, Certainty in Heisenberg's uncertainty principle: Revisiting definitions for estimation errors and disturbance, Phys. Rev. A **89**, 022106 (2014).

[28] B. Yadin, M. Fadel, and M. Gessner, Metrological complementarity reveals the Einstein-Podolsky-Rosen paradox, Nat. Commun. **12**, 2410 (2021).

[29] A. Shaji and C. M. Caves, Qubit metrology and decoherence, Phys. Rev. A **76**, 032111 (2007).

[30] J. Ma, X. Wang, C. Sun, and F. Nori, Quantum spin squeezing, Phys. Rep. **509**, 89 (2011).

[31] G. Tóth and I. Apellaniz, Quantum metrology from a quantum information science perspective, J. Phys. A: Math. Theor. **47**, 424006 (2014).

[32] D. R. M. Arvidsson-Shukur, N. Y. Halpern, H. V. Lepage, A. A. Lasek, C. H. W. Barnes, and S. Lloyd, Quantum advantage in postselected metrology, Nat. Commun. **11**, 3775 (2020).

[33] J. J. Meyer, J. Borregaard, and J. Eisert, A variational toolbox for quantum multi-parameter estimation, npj Quantum Inf. **7**, 89 (2021).

[34] I. Gianani, V. Berardi, and M. Barbieri, Witnessing quantum steering by means of the fisher information, Phys. Rev. A **105**, 022421 (2022).

[35] K. Chabuda, J. Dziarmaga, T. J. Osborne, and R. Demkowicz-Dobrzański, Tensor-network approach for quantum metrology in many-body quantum systems, Nat. Commun. **11**, 250 (2020).

[36] L. J. Fiderer, J. Schuff, and D. Braun, Neural-network heuristics for adaptive bayesian quantum estimation, PRX Quantum **2**, 020303 (2021).

[37] S. Zhou and L. Jiang, Asymptotic theory of quantum channel estimation, PRX Quantum **2**, 010343 (2021).

[38] K. Xu, Y.-R. Zhang, Z.-H. Sun, H. Li, P. Song, Z. Xiang, K. Huang, H. Li, Y.-H. Shi, C.-T. Chen, X. Song, D. Zheng, F. Nori, H. Wang, and H. Fan, Metrological characterization of nongaussian entangled states of superconducting qubits, Phys. Rev. Lett. **128**, 150501 (2022).

[39] M. Yu, Y. Liu, P. Yang, M. Gong, Q. Cao, S. Zhang, H. Liu, M. Heyl, T. Ozawa, N. Goldman, and J. Cai, Quantum Fisher information measurement and verification of the quantum cramér–rao bound in a solid-state qubit, npj Quantum Inf. **8**, 56 (2022).

[40] A. Fallani, M. A. C. Rossi, D. Tamascelli, and M. G. Genoni, Learning feedback control strategies for quantum metrology, PRX Quantum **3**, 020310 (2022).

[41] V. Giovannetti, S. Lloyd, and L. Maccone, Quantum metrology, Phys. Rev. Lett. **96**, 010401 (2006).

[42] B. M. Escher, R. L. de Matos Filho, and L. Davidovich, General framework for estimating the ultimate precision limit in noisy quantum-enhanced metrology, Nat. Phys. **7**, 406 (2011).

[43] V. Giovannetti, S. Lloyd, and L. Maccone, Advances in quantum metrology, Nat. Photon. **5**, 222 (2011).

[44] R. Demkowicz-Dobrzański and L. Maccone, Using entanglement against in quantum metrology, Phys. Rev. Lett. **113**, 250801 (2014).

[45] A. Strikis, D. Qin, Y. Chen, S. C. Benjamin, and Y. Li, Learning-based quantum error mitigation, PRX Quantum **2**, 040330 (2021).

[46] B. Regula and R. Takagi, Fundamental limitations on distillation of quantum channel resources, Nat. Commun. **12**, 4411 (2021).

[47] C. J. Myatt, B. E. King, Q. A. Turchette, C. A. Sackett, D. Kielpinski, W. M. Itano, C. Monroe, and D. J. Wineland, Decoherence of quantum superpositions through coupling to engineered reservoirs, Nature (London) **403**, 269 (2000).

[48] P. D. Nation, H. Kang, N. Sundaresan, and J. M. Gambetta, Scalable mitigation of measurement errors on quantum computers, PRX Quantum **2**, 040326 (2021).

[49] D. F. Wise, J. J. L. Morton, and S. Dhomkar, Using deep learning to understand and mitigate the qubit noise environment, PRX Quantum **2**, 010316 (2021).

[50] G. Chiribella and H. Kristjánsson, Quantum Shannon theory with superpositions of trajectories, Proc. R. Soc. A: Math. Phys. Eng. Sci. **475**, 20180903 (2019).

[51] A. A. Abbott, J. Wechs, D. Horsman, M. Mhalla, and C. Branciard, Communication through coherent control of quantum channels, Quantum **4**, 333 (2020).

[52] K. Goswami, Y. Cao, G. A. Paz-Silva, J. Romero, and A. G. White, Increasing communication capacity via superposition of order, Phys. Rev. Res. **2**, 033292 (2020).

[53] G. Chiribella, M. Wilson, and H. F. Chau, Quantum and classical data transmission through completely depolarizing channels in a superposition of cyclic orders, Phys. Rev. Lett. **127**, 190502 (2021).

[54] S. Slussarenko, M. M. Weston, L. K. Shalm, V. B. Verma, S.-W. Nam, S. Kocsis, T. C. Ralph, and G. J. Pryde, Quantum channel correction outperforming direct transmission, Nat. Commun. **13**, 1832 (2022).

[55] D. K. L. Oi, Interference of quantum channels, Phys. Rev. Lett. **91**, 067902 (2003).

[56] N. Gisin, N. Linden, S. Massar, and S. Popescu, Error filtration and entanglement purification for quantum communication, Phys. Rev. A **72**, 012338 (2005).

[57] G. Rubino, L. A. Rozema, D. Ebler, H. Kristjánsson, S. Salek, P. Allard Guérin, Č. Brukner, A. A. Abbott, C. Branciard, G. Chiribella, and P. Walther, Experimental quantum communication enhancement by superposing trajectories, Phys. Rev. Res. **3**, 013093 (2021).

[58] A. Kandala, A. Mezzacapo, K. Temme, M. Takita, M. Brink, J. M. Chow, and J. M. Gambetta, Hardware-efficient variational quantum eigen-

solver for small molecules and quantum magnets, Nature (London) **549**, 242 (2017).

[59] G. García-Pérez, M. A. C. Rossi, and S. Maniscalco, IBM Q experience as a versatile experimental testbed for simulating open quantum systems, npj Quantum Inf. **6**, 1 (2020).

[60] S.-N. Sun, M. Motta, R. N. Tazhigulov, A. T. Tan, G. K.-L. Chan, and A. J. Minnich, Quantum computation of finite-temperature static and dynamical properties of spin systems using quantum imaginary time evolution, PRX Quantum **2**, 010317 (2021).

[61] C. Berke, E. Varvelis, S. Trebst, A. Altland, and D. P. DiVincenzo, Transmon platform for quantum computing challenged by chaotic fluctuations, Nat. Commun. **13**, 2495 (2022).

[62] S. L. Braunstein and C. M. Caves, Statistical distance and the geometry of quantum states, Phys. Rev. Lett. **72**, 3439 (1994).

[63] K. C. Tan, V. Narasimhachar, and B. Regula, Fisher information universally identifies quantum resources, Phys. Rev. Lett. **127**, 200402 (2021).

[64] W. F. Stinespring, Positive functions on C^*-algebras, Proc. Amer. Math. Soc. **6**, 211 (1955).

[65] K. Kraus, A. Böhm, J. D. Dollard, and W. H. Wootters, eds., *States, Effects, and Operations Fundamental Notions of Quantum Theory* (Springer Berlin Heidelberg, 1983).

[66] M. M. Wilde, *Quantum Information Theory* (Cambridge University Press, 2017).

[67] Y.-N. Chen, C.-M. Li, N. Lambert, S.-L. Chen, Y. Ota, G.-Y. Chen, and F. Nori, Temporal steering inequality, Phys. Rev. A **89**, 032112 (2014).

[68] K. Bartkiewicz, A. Černoch, K. Lemr, A. Miranowicz, and F. Nori, Temporal steering and security of quantum key distribution with mutually unbiased bases against individual attacks, Phys. Rev. A **93**, 062345 (2016).

[69] S.-L. Chen, N. Lambert, C.-M. Li, A. Miranowicz, Y.-N. Chen, and F. Nori, Quantifying non-Markovianity with temporal steering, Phys. Rev. Lett. **116**, 020503 (2016).

[70] C.-M. Li, Y.-N. Chen, N. Lambert, C.-Y. Chiu, and F. Nori, Certifying single-system steering for quantum-information processing, Phys. Rev. A **92**, 062310 (2015).

[71] S.-J. Xiong, Y. Zhang, Z. Sun, L. Yu, Q. Su, X.-Q. Xu, J.-S. Jin, Q. Xu, J.-M. Liu, K. Chen, and C.-P. Yang, Experimental simulation of a quantum channel without the rotating-wave approximation: testing quantum temporal steering, Optica **4**, 1065 (2017).

[72] C.-Y. Huang, N. Lambert, C.-M. Li, Y.-T. Lu, and F. Nori, Securing quantum networking tasks with multipartite einstein-podolsky-rosen steering,

Phys. Rev. A **99**, 012302 (2019).

[73] IBM Quantum Services, https://quantum-computing.ibm.com/services?services=systems [May. 2022].

[74] J. Johansson, P. Nation, and F. Nori, QuTiP: An open-source python framework for the dynamics of open quantum systems, Comput. Phys. Commun. **183**, 1760 (2012).

[75] J. Johansson, P. Nation, and F. Nori, QuTiP 2: A python framework for the dynamics of open quantum systems, Comput. Phys. Commun. **184**, 1234 (2013).

[76] B. Li, S. Ahmed, S. Saraogi, N. Lambert, F. Nori, A. Pitchford, and N. Shammah, Pulse-level noisy quantum circuits with QuTiP, Quantum **6**, 630 (2022).

[77] H.-Y. Ku, N. Lambert, F.-J. Chan, C. Emary, Y.-N. Chen, and F. Nori, Experimental test of non-macrorealistic cat states in the cloud, npj Quantum Inf. **6**, 98 (2020).

[78] Z.-P. Yang, H.-Y. Ku, A. Baishya, Y.-R. Zhang, A. F. Kockum, Y.-N. Chen, F.-L. Li, J.-S. Tsai, and F. Nori, Deterministic one-way logic gates on a cloud quantum computer, Phys. Rev. A **105**, 042610 (2022).

[79] G. Lindblad, On the generators of quantum dynamical semigroups, Commun. Math. Phys. **48**, 119 (1976).

[80] E. Magesan, J. M. Gambetta, and J. Emerson, Scalable and robust randomized benchmarking of quantum processes, Phys. Rev. Lett. **106**, 180504 (2011).

[81] E. Magesan, J. M. Gambetta, and J. Emerson, Characterizing quantum gates via randomized benchmarking, Phys. Rev. A **85**, 042311 (2012).

[82] M. Urbanek, B. Nachman, V. R. Pascuzzi, A. He, C. W. Bauer, and W. A. de Jong, Mitigating depolarizing noise on quantum computers with noise-estimation circuits, arXiv:2103.08591 (2021).

[83] D. Ebler, S. Salek, and G. Chiribella, Enhanced communication with the assistance of indefinite causal order, Phys. Rev. Lett. **120**, 120502 (2018).

[84] J. Barrett, R. Lorenz, and O. Oreshkov, Cyclic quantum causal models, Nat. Commun. **12**, 885 (2021).

[85] G. Chiribella and X. Zhao, Heisenberg-limited metrology with coherent control on the probes' configuration, arXiv:2206.03052 (2022).

[86] M. A. Nielsen and I. L. Chuang, *Quantum Computation and Quantum Information: 10th Anniversary Edition* (Cambridge University Press, 2011).

[87] K. Michielsen, M. Nocon, D. Willsch, F. Jin, T. Lippert, and H. De Raedt, Benchmarking gate-based quantum computers, Comput. Phys. Commun. **220**, 44 (2017).

[88] A. Fedorov, L. Steffen, M. Baur, M. P. da Silva, and A. Wallraff, Implementation of a Toffoli gate with superconducting circuits, Nature (London) **481**, 170 (2011).